Energy and vibrational spectrum of the Si(111) (7×7) surface from empirical potentials

X.-P. Li, G. Chen, and P. B. Allen
Department of Physics, State University of New York at Stony Brook, Stony Brook, New York 11794-3800

J. Q. Broughton
Department of Materials Science, State University of New York at Stony Brook, Stony Brook, New York 11794-2275
(Received 4 January 1988)

The stability and vibrational properties of the Si(111) (7×7) [Takayanagi, or dimer-adatom-stacking-fault structure (DAS)] surface are investigated using the Stillinger-Weber and modified Tersoff interatomic potentials for silicon. The diamond-cubic bulk and surface-terminated bulk and $(\sqrt{3}\times\sqrt{3})$ structures are treated for comparison. The modified Tersoff potential underestimates the bulk transverse-acoustic branch frequencies while the Stillinger-Weber does the opposite. Both potentials produce z expansions away from the idealized (constant-bond-length) structures. The Stillinger-Weber potential produces surface energies in the following order: terminated bulk $<(\sqrt{3}\times\sqrt{3})<(7\times7)$ DAS, whereas the modified Tersoff potential reverses this order in accord with local-density-functional calculations and experiment. The two potentials produce surprisingly similar features in the local densities of vibrational states on surface atoms. In the case of adatoms, a high-frequency state split off from the bulk continuum and a mid-frequency state are observed. The high-frequency state has significant weight in the z direction on the adatom, (x,y) weight (only) on the three first-layer atoms to which the adatom is attached, and z weight again on the second- and third-layer atoms directly beneath; the mid-frequency state corresponds to the z motion of the adatom and the two atoms underneath in phase with each other, while out of phase with the three first-layer atoms attached which symmetrically vibrate in the (x,y) plane as well. Atoms with dangling bonds (first-layer atoms not directly attached to adatoms and atoms in the open site at the corners of the unit cell) have small force constants in the z direction and their local spectra only exhibit weight at low frequencies. The z-polarized adatom vibrations agree nicely with recent inelastic electron-energy-loss spectra by Daum, Ibach, and Müller.

I. INTRODUCTION

The Si(111) surface has proved a rich subject for experiment and theory. The early scanning-tunneling-microscope (STM) experiments of Binnig *et al.*[1] revealed the presence of 12 adatoms per surface (7×7) unit cell. This observation was put in context by Takayanagi *et al.*,[2] who used transmission electron diffraction to derive the dimer-adatom-stacking-fault (DAS) model for the positions of atoms in the (7×7) cell. This model was also derived from the glancing-incidence x-ray-diffraction experiments of Robinson *et al.*[3] The recent STM work of Hamers *et al.*[4] and of Becker *et al.*[5] further corroborated the DAS structure.

That adatoms are an important feature in the (7×7) unit cell was first proposed by Harrison.[6] The adatoms reduce the density of surface dangling bonds. Since then, local-density-functional total-energy pseudopotential calculations including atom-positional relaxation have been performed on Al,[7] In,[8] Ge,[9] and Si (Ref. 10) adatoms on threefold hollow surface sites to determine whether the adatoms prefer to "sit" above second-layer (T, or "top") or fourth-layer (H, or "hollow") substrate atoms. These calculations placed adatoms in a $(\sqrt{3}\times\sqrt{3})$ layer above a truncated bulk and each showed the T site to be preferred. An earlier (2×2) adatom calculation had shown the H site to be preferred, but full-geometry optimization had not been performed on the T system.[11] Recently, such optimization has been performed and the T site found to be degenerate with the H.[12] These results are significant since the local adatom environment of the (7×7) DAS model is similar to the (2×2) and to the $(\sqrt{3}\times\sqrt{3})$ models. The consensus of opinion is that adatoms in the (7×7) structure adopt T-site positions.[13]

The other features of the DAS model are the dimers along the edges of the unit cell (see Fig. 1) and along the line joining the wide-angle apexes of the unit cell. The latter separate the stacking-faulted (left) triangle from the unfaulted (right) triangle of the unit cell. This arrangement produces 42 first-layer atoms, rather than the 49 of the simple terminated bulk, which further reduces the number of surface dangling bonds. Qian and Chadi[13] studied the dimer and stacking-fault contributions to the surface energy using the Keating model,[14] a potential devised to describe small distortions of covalent systems away from tetrahedrality. Together with results of Nothrup's local-density-functional calculations for adatom absorption energies,[10] they were able to show that of the sequence of generalized (5×5), (7×7), (9×9), and (11×11) DAS models the (7×7) structure had the lowest energy. In a later paper, Qian and Chadi[13] used an appropriately parametrized tight-binding Hamiltonian specific to the DAS model to relax the contents of the unit cell. They were able to examine the (5×5) and

(7×7) structures and again found the (7×7) more stable. Vanderbilt[15] argued convincingly that the driving force for the (7×7) DAS reconstruction is the domain walls (dimer rows). He showed that the adatoms play only an incidental role because the (7×7) DAS reconstruction is energetically favorable even without them. He studied the stresses on various Si(111) surfaces and ruled out the relief of compressive stress as the driving force. He was able to show that the Si(111) surface has the (7×7) DAS structure, whereas the Ge(111) surface has the $c(2\times8)$ structure, and to explain the trend $c(2\times8)\rightarrow(7\times7)$ DAS$\rightarrow(5\times5)$ DAS with compression of the surface layer.

Recently, several interatomic potentials have been proposed[16–23] which attempt to describe the energy hypersurface of ensembles of silicon atoms. The Stillinger-Weber,[16] Tersoff I,[17] Tersoff II,[18] and Brenner and Garrison[19] potentials all successfully give dimerization of the Si(100) surface. The Pearson-Takai-Halicioglu-Tiller potential[20] has been used to describe the unreconstructed and (2×1) reconstructed Si(111) surface. In this paper we examine the ability of the Stillinger-Weber[16] and Tersoff II (Ref. 18) potentials to describe the (7×7) structure of the Si(111) surface. This is perhaps the severest test to which these potentials can be put. Specifically, we calculate surface coordinates and energies for various relaxed structures, and also local vibrational densities of states (LDOS's),

$$F(l,\alpha,\omega)=\sum_i |\varepsilon_i(l,\alpha)|^2\delta(\omega-\omega_i)\ , \tag{1}$$

where $\varepsilon_i(l,\alpha)$ is the α component of the polarization vector of the ith mode (of frequency ω_i) on atom l. We examine $F(l,\alpha,\omega)$ for several types of surface atoms. Both potentials yield a high-frequency split-off mode and a mid-frequency mode of z polarization on the adatoms, agreeing nicely with recent electron-energy-loss spectra (EELS) of Daum *et al.*[24]

In the following section we describe the Stillinger-Weber and Tersoff II potentials. In Sec. III we describe the energies and atomic arrangements of the relaxed $(\sqrt{3}\times\sqrt{3})$ and (7×7) structures, while in Sec. IV we present the vibrational densities of states for both the bulk diamond-cubic and the (7×7) surface structures. In Sec. V we present our conclusions.

II. POTENTIALS

The Stillinger-Weber (SW) potential[16] was designed to describe bulk crystal and liquid phases of silicon. It gives the correct melting temperature[25] and produces a liquid structure factor similar to experiment. There is no consensus as to whether it can describe the amorphous phase;[25–27] our work suggests that it cannot.[25] The SW potential is of short-ranged three-body form, the exact many-body expansion for the total energy of the system being truncated after the three-body term. In contrast, the Tersoff I (Ref. 17) and II (Ref. 18) potentials do not rely upon this expansion and are, in fact, N-body, but short-ranged, potentials. Tersoff chose to generalize the simple pairwise Morse potential in such a way that interaction between pairs is environment dependent. The parameters of his model are fitted to bulk diamond-cubic, simple-cubic, and face-centered-cubic properties, and also to the cohesive energy of the Si dimer. The potentials give cohesive energies and lattice parameters for the β-tin structure of Si in close agreement with the *ab initio* calculations of Yin and Cohen.[28] The Tersoff I potential predicts the T-site adatom in the $(\sqrt{3}\times\sqrt{3})$ structure of Si(111) to be more stable than the H-site one, in accord with Northrup's *ab initio* results. Further, the DAS model of the (7×7) reconstruction is found to be lower in energy than rival structures. However, we use the modified Tersoff II potential with somewhat different properties, which will be described below.

The SW potential represents the total potential energy (PE), $V_{\rm tot}$ of the system as a sum over all pairs of atoms of two- and three-body terms:

$$V_{\rm tot}=A\sum_{\substack{i,j\\(i>j)}}(Br_{ij}^{-p}-r_{ij}^{-q})\exp[(r_{ij}-a_0)^{-1}] +\lambda\sum_{\substack{i,j,k\\(i>j>k)}}\exp[\gamma(r_{ij}-a_0)^{-1} +\gamma(r_{ik}-a_0)^{-1}](\cos\theta_{jik}+\tfrac{1}{3})^2\ . \tag{2}$$

The first term vanishes if the distance between i and j (r_{ij}) is greater than a_0. The second term vanishes if either r_{ij} or r_{ik} is greater than a_0. The cosine term (where θ represents the angle at the apex of the triplet) goes to zero at the tetrahedral angle.

Tersoff writes the total PE as the sum over all pairs of the Morse-like interaction:

$$V_{\rm tot}=\tfrac{1}{2}\sum_{\substack{i,j\\(i\neq j)}}f_c(r_{ij})[A\exp(-\lambda_1 r_{ij})-B_{ij}\exp(-\lambda_2 r_{ij})]\ , \tag{3}$$

where f_c is a cutoff function to restrict the range of interaction. A crucial point is that B_{ij} depends on the local environment of the ij bond. Tersoff's original paper[17] (Tersoff I) gave an analytic expression for B and it was this potential which did well in describing β-tin Si and the $(\sqrt{3}\times\sqrt{3})$ structures of Si(111). However, it has since been shown[29] that this representation of the potential energy gave the wrong ground state (i.e., not diamond cubic) for the bulk, and we therefore chose to use the more recent parametrization[18] (Tersoff II), which uses a different functional form for B_{ij}:

$$B_{ij}=B_0[1+b(Z_{ij})^n]^{-1/2n}\ , \tag{4}$$

$$Z_{ij}=\sum_{k\,(\neq i,j)}f_c(r_{ik})g(\theta_{jik})\exp\{[-\lambda_3(r_{ik}-r_{ij})]^3\}\ , \tag{5}$$

where

$$g(\theta)=1+\frac{c^2}{d^2}-\frac{c^2}{d^2+(\cos\theta+h)^2}\ , \tag{6}$$

TABLE I. Parameter values for the Tersoff II potential [Eqs. (3)–(7)].

R	3.0 Å
D	0.2 Å
B_0	95.3727
A	3264.65
λ_1	3.239 40
λ_2	1.325 83
b	$1.409\,49\times10^{-11}$
n	22.9559
c	4.838 10
d	2.041 67
h	$8.804\,98\times10^{-6}$
λ_3	1.325 83

$$f_c(r)=\begin{cases}1, & r<R-D\\ \frac{1}{2}\left[1-\sin\left[\frac{\pi(r-R)}{2D}\right]\right], & R-D<r<R+D\\ 0, & r>R+D\ .\end{cases} \tag{7}$$

The values of the parameters in Eqs. (3)–(7) are given in Table I. The potential now does have the correct zero-pressure ground state for bulk silicon. The SW potential is actually of slightly larger range than the Tersoff II potential.

III. SURFACE STRUCTURAL ENERGIES

We employed a steepest-descent method to relax the surface structures, which were represented as slabs with periodic boundary conditions (nearest-image convention) in the (x,y) plane. The (111) DAS systems comprise 12 adatoms, a 42-atom first layer, a 48-atom second layer, and one-and-a-half 98-atom double layers: the whole of this is duplicated in the other half of the slab in such a manner that the system possesses a center of inversion. A top view is shown in Fig. 1. The adatoms and first two double layers were allowed to dynamically relax in the field of static "bulk" double layers. The (x,y) box-size dimension was obtained from the $T=0$ minimum-potential-energy bulk lattice parameter of each potential. (The Tersoff potential gives the same nearest-neighbor distance, 2.352 Å, as experiment at room temperature, and the SW potential gives 2.350 Å.)

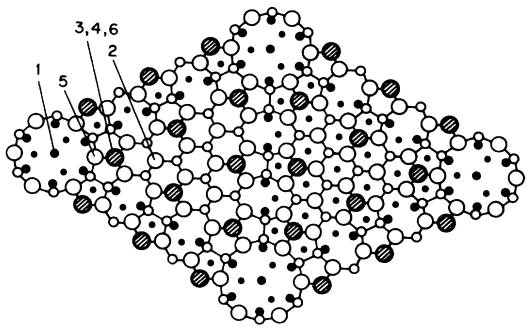

FIG. 1. Top view of the Takayanagi, or DAS, model of the Si(111) (7×7) surface (taken from Ref. 13). The numbers denote atoms whose local vibrations are shown in Figs. 7–12. Atom number 4 is beneath the adatom denoted by 3 and atom 6 is beneath atom 4. (Adatoms are shaded; deeper atoms are solid dots.)

TABLE II. Surface energies [eV/(10² Å)] of different Si surfaces.

	SW potential	Tersoff II potential
Si(111)		
terminated bulk	8.49	5.50
$(\sqrt{3}\times\sqrt{3})$ H	11.24	4.42
$(\sqrt{3}\times\sqrt{3})$ T	13.35	4.70
(7×7) DAS	12.48	4.27
Si(100)		
terminated bulk	14.71	
$p(2\times1)$	9.00	
$c(2\times2)$	9.47	

In Table II we present our relaxed surface energies. The SW potential completely reverses the order of stability from that expected from Northrup's *ab initio* calculations[10] and experiment. The Tersoff II potential has the (7×7) structure more stable than either the terminated bulk or the $(\sqrt{3}\times\sqrt{3})$ structures. Both the Tersoff II and SW potentials predict the $(\sqrt{3}\times\sqrt{3})$ H structure to be more stable than the T structure, in contradiction with Northrup's results. Clearly, the SW potential is quite unrealistic, and the Tersoff potential is more nearly reasonable for the (111) surface. However, on the Si(100) surface the SW potential does produce a more stable dimer reconstruction than the simple terminated bulk, as found also by Weber[30] and others.[31]

In Table III we give the relaxed z positions of the top few layers of the $(\sqrt{3}\times\sqrt{3})$ reconstructions. Figure 2 shows the surface computational cells and the atom-

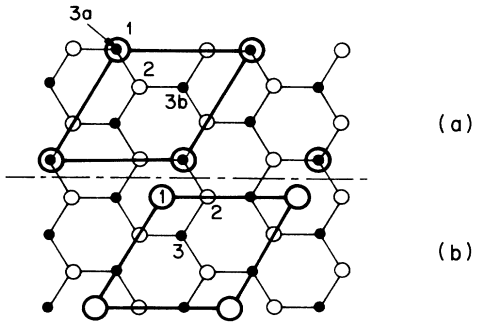

FIG. 2. The $(\sqrt{3}\times\sqrt{3})$ "top" (T) and "hollow" (H) structures are shown in (a) and (b), respectively.

TABLE III. z shifts in Å from ideal (constant-bond-length) $(\sqrt{3}\times\sqrt{3})$ surface.

Atom	Northrup	SW potential	Tersoff II potential
$(\sqrt{3}\times\sqrt{3})$ *H*			
1	0.47	0.82	0.50
2	−0.14	0.10	0.11
3	−0.08	0.00	−0.01
$(\sqrt{3}\times\sqrt{3})$ *T*			
1	0.53	1.13	0.53
2	−0.08	0.15	0.13
3*a*	−0.39	−0.33	−0.30
3*b*	0.09	0.19	0.13

numbering scheme (due to Northrup[10]). The SW potential produces much greater relaxation than does the Tersoff II potential. Both produce a buckling in the second layer for the T structure such that the atom directly below the adatom goes down while the others move up. Northrup's results also bear this out. As we shall see later, such buckling is not observed in either our DAS structures or in those due to Qian and Chadi.[13] When taken in conjunction with Table IV (which shows the nearest-neighbor separations), we note that the Tersoff II potential produces interatomic distances more in accord with those of Northrup.

Compare now Tables III and IV with Tables V and VI, which show the relaxed z displacements and bond lengths of atoms in the top few layers of the (7×7) DAS model. Again, we note that the SW potential produces very large z shifts for the adatoms, whereas the Tersoff II potential is similar to that of Qian and Chadi. In fact, the magnitude of these shifts and the adatom-to-substrate bond lengths in the calculations of Qian and Chadi are very similar to those predicted from Northrup's $(\sqrt{3}\times\sqrt{3})$ T-site *ab initio* results.[10] [In each triplet of results in Table VI, the first two rows correspond to the 1-2 distances of the $(\sqrt{3}\times\sqrt{3})$ T-site structure. The third row corresponds to the 1-3*a* distance.]

In Table V the signs of the z shifts of the three different calculations do not correlate in the first layer but do in the second. The positions of the atoms on the faulted side are almost identical with the equivalent ones on the unfaulted side of the unit cell in the Tersoff II and SW structures. This is less true in the tight-binding calculations. However, Table VI shows that the interatomic distances between an adatom and its nearest neighbors in the tight-binding calculations are remarkably constant over the unit cell. The Tersoff II interatomic distances are a little smaller and more variable than the tight-binding calculations, whereas the SW distances are all uniformly larger than those of Qian and Chadi.

TABLE IV. Nearest-neighbor distances in Å of relaxed $(\sqrt{3}\times\sqrt{3})$ system.

Atom pair	Northrup	SW potential	Tersoff II potential
$(\sqrt{3}\times\sqrt{3})$ *H*			
1-2	2.55	2.58	2.40
1-3	3.05	3.31	3.09
$(\sqrt{3}\times\sqrt{3})$ *T*			
1-2	2.49	2.73	2.42
1-3*a*	2.49	3.03	2.39

TABLE V. z shifts in Å from ideal (constant-bond-length) DAS model. Column 1 is the numbering system of Ref. 13, while numbers in parentheses refer to the numbering system of Fig. 1.

Atom	Qian-Chadi	SW potential	Tersoff II potential
1 (3)	0.50	1.13	0.51
2	0.42	1.12	0.52
3	0.41	1.12	0.52
4	0.44	1.12	0.50
5 (5)	−0.05	0.13	−0.05
6	−0.03	0.19	0.16
7 (2)	0.29	0.06	−0.15
8	−0.13	0.16	0.19
9	−0.08	0.14	0.08
10	−0.09	0.14	0.08
11	−0.10	0.16	0.18
12	0.30	0.06	−0.16
13	−0.06	0.18	0.16
14	−0.09	0.12	−0.06
15 (4)	−0.42	−0.32	−0.30
16	−0.07	0.05	0.05
17	−0.08	0.04	0.03
18	0.04	0.17	0.11
19	0.05	0.16	0.12
20	−0.47	−0.32	−0.29
21	−0.07	0.02	0.03
22	−0.47	−0.32	−0.30
23	0.06	0.16	0.12
24	0.06	0.17	0.12
25	−0.45	−0.34	−0.31

TABLE VI. Nearest-neighbor distances in Å of relaxed DAS model (numbering system of Ref. 13).

Atom pair	Qian-Chadi	SW potential	Tersoff II potential
1-5	2.48	2.67	2.39
1-6	2.48	2.73	2.42
1-15	2.48	3.02	2.38
2-8	2.48	2.77	2.44
2-9	2.48	2.72	2.41
2-20	2.46	3.01	2.39
3-11	2.48	2.77	2.44
3-10	2.47	2.71	2.41
3-22	2.46	3.01	2.39
4-14	2.47	2.67	2.39
4-13	2.48	2.73	2.42
4-25	2.46	3.02	2.38

IV. VIBRATIONAL PROPERTIES

A. Bulk modes

Broughton and Li[25] evaluated the phase diagram of SW silicon by following crystal-vapor coexistence and equating the chemical potentials of the crystal and liquid phases. One of their reference states was the harmonic $T=0$ crystal. In Figs. 3 and 4 we reproduce their dispersion curves and density of states (DOS). Second derivatives of the potential energy required for the dynamical matrix were obtained analytically. The density chosen for the calculation was that which gives minimum energy at $T=0$, i.e., a number density of 4.994×10^{22} atoms cm^{-3}. Note that the spectrum extends to higher frequency than experiment and that the transverse-acoustic branch near the Brillouin-zone boundaries is obtained with less accuracy than the longitudinal branch. The DOS structure agrees reasonably well with results of calculations[32] fitted to experiment. Also shown in Fig. 4 is a histogram DOS derived from the present calculation for the (7×7) structure. This represents the LDOS on an atom near the middle of our 498-atom computational slab, i.e., derived from Eq. (1) by summing α over x, y, and z. In the histogram calculation, the wave vector (Q) parallel to the slab is a well-defined quantum number, but we use only the Q=0 eigenvalues. The (7×7) cell is sufficiently large that little new information would emerge from a calculation which summed over Q. Translational symmetry has little effect except to allow low-energy electron-diffraction (LEED) patterns to be measured. The close correspondence between the (7×7) histogram and the bulk tetrahedral calculations confirms this observation and justifies our use of Q=0 eigenstates only in subsequent calculations.

The bulk spectra of the Tersoff II potential were obtained in a slightly different manner. Second derivatives of the potential with respect to displacement were obtained by numerically differentiating the analytically obtained first derivatives. (Second derivatives of the Tersoff II potential are not easy to handle analytically.) Figures 5 and 6 present the dispersion curves and bulk DOS of

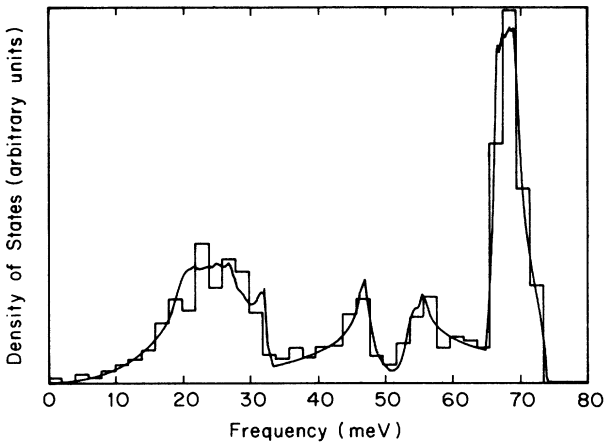

FIG. 4. Bulk-Si-phonon density of states vs frequency from the SW potential. The solid line is a tetrahedron calculation and the histogram is an interior-atom LDOS from a (7×7) slab calculation.

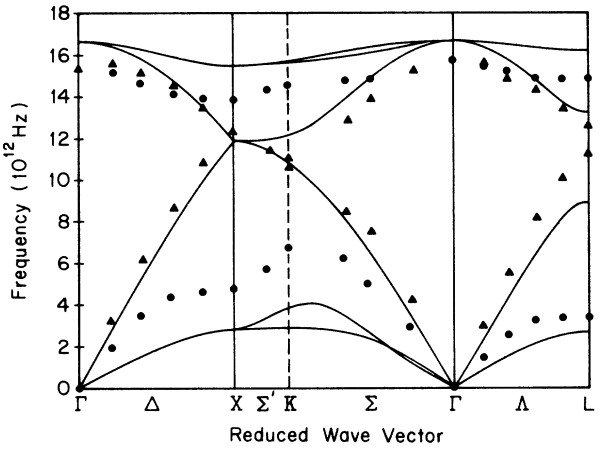

FIG. 5. Same as Fig. 3, for the Tersoff II potential.

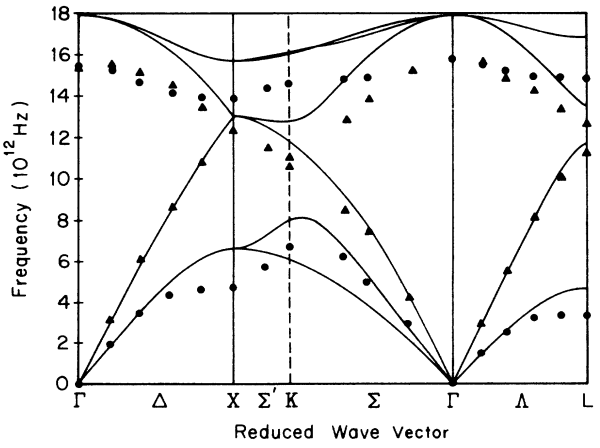

FIG. 3. Bulk-Si-phonon dispersion curves from the SW potential compared with experiment.

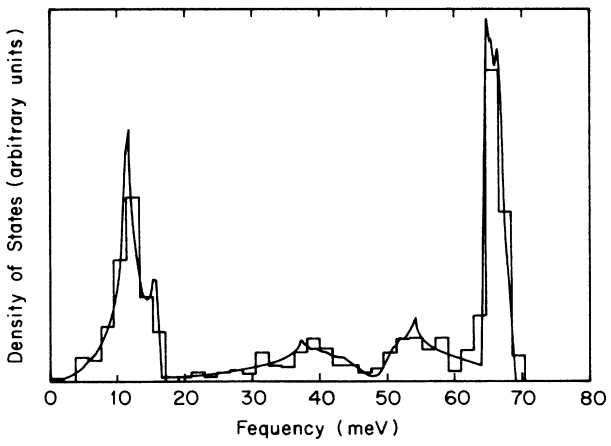

FIG. 6. Same as Fig. 4, for the Tersoff II potential.

the Tersoff II potential. Again, the width of the spectrum is larger than experiment. The fit to experiment of the dispersion curve is, in general, poorer than that of the SW potential. Further, the transverse-acoustic–mode frequencies are now underestimated in contrast to the situation found for the SW potential. The broad, flat transverse-acoustic branch produces a much sharper feature in the low-frequency region of the density of states than is found experimentally. Thus, it seems that although the Tersoff II potential seems to give more reliable silicon structures when compared with first-principles theories, its frequencies are in poorer accord with experiment than the SW potential. The interior atom (7×7) $\mathbf{Q}=\mathbf{0}$ histogram is also shown in Fig. 6, and agrees nicely with the bulk results.

B. Surface modes

For the purposes of discussing LDOS on atoms in the surface region, we can distinguish eight categories of atoms: (1) adatoms, (2) first-layer atoms directly attached to adatoms, (3) first-layer atoms not attached. (4) second-layer atoms directly below adatoms, (5) second-layer atoms not below, (6) second-layer dimers, (7) third-layer atoms directly below adatoms, and (8) "bulk" atoms.

The most immediate generalization to be made is that atoms which would be equivalent across the unit cell if it were not for the fact that one side is faulted and the other not do have almost identical LDOS's. Thus (for example), of the four symmetrically inequivalent adatoms in the (7×7) DAS cell, although all four exhibit very similar spectral features, those which map into each other by the (inexact) reflection across the dimer chains are much more nearly identical than are spectra of inequivalent adatoms on the same triangular patch.

"Bulk" atoms are, for our purposes, those which lie deeper than second layer, except the third-layer atoms directly below adatoms. The atoms here have LDOS's extremely close to the bulk, as shown in Figs. 4 and 6. Further, for both the SW and Tersoff II potentials, atoms in the second layer not directly below adatoms and even the dimer atoms which "stitch" the faulted and unfaulted regions together have LDOS's which are very similar to those of the bulk. There is but one exception here, the LDOS of atom 1 (see Fig. 1), which lies in the third layer in the open site at the corners of the DAS unit cell and has a dangling bond. The LDOS of atom 1 is shown in Fig. 7. Both potentials give extremely similar spectra and show the z component to be weighted to the low-frequency end, just as atom 2 does.

Atom 2 is one of the first-layer atoms not directly attached to adatoms and therefore has a dangling bond. Figure 8 presents its spectra. The similarities of the SW and Tersoff II results are again striking. In both cases, the x and y components have narrow resonances near 66 meV, but with some broader weight near 15 meV. The z component, by contrast, has all of its weight at low frequencies. The only dissimilarities are those of frequency scale and of mid-frequency (i.e., 25–45 meV) intensity. These dissimilarities are found also in the bulk DOS. The high-frequency cutoff of the SW bulk system (Figs. 3 and 4) is higher than that of the Tersoff II system (Figs. 5 and 6). Employing the same sliding scale that brings bulk fre-

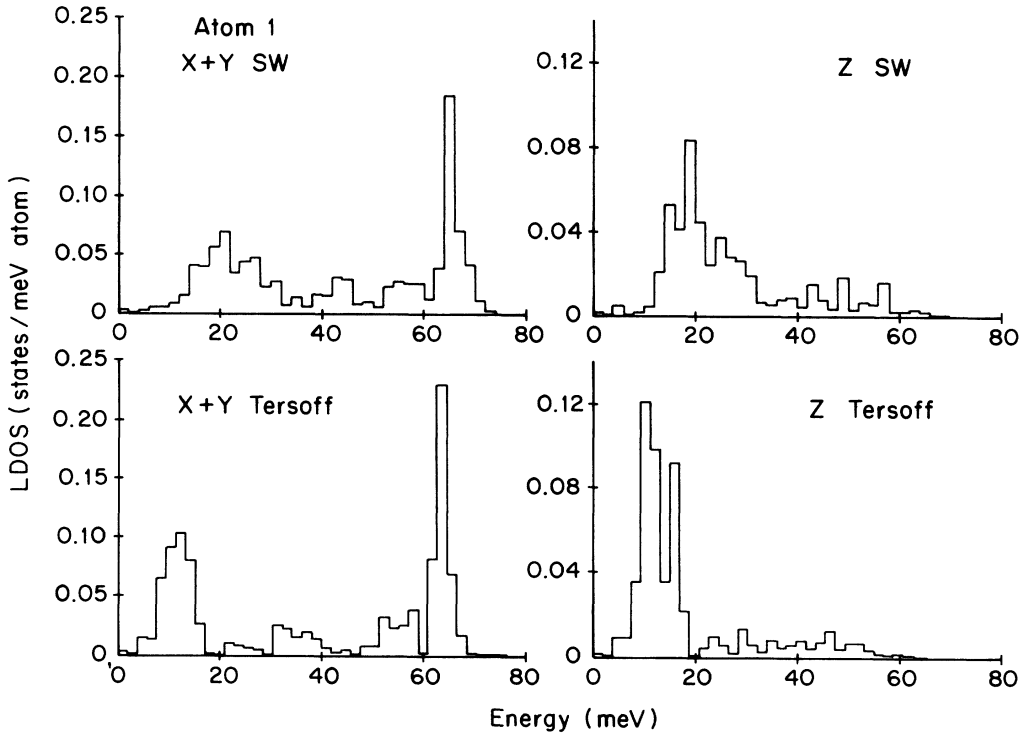

FIG. 7. LDOS for atom 1 of Fig. 1, showing z-polarized and (x,y)-polarized vibrations calculated from SW and Tersoff II potentials.

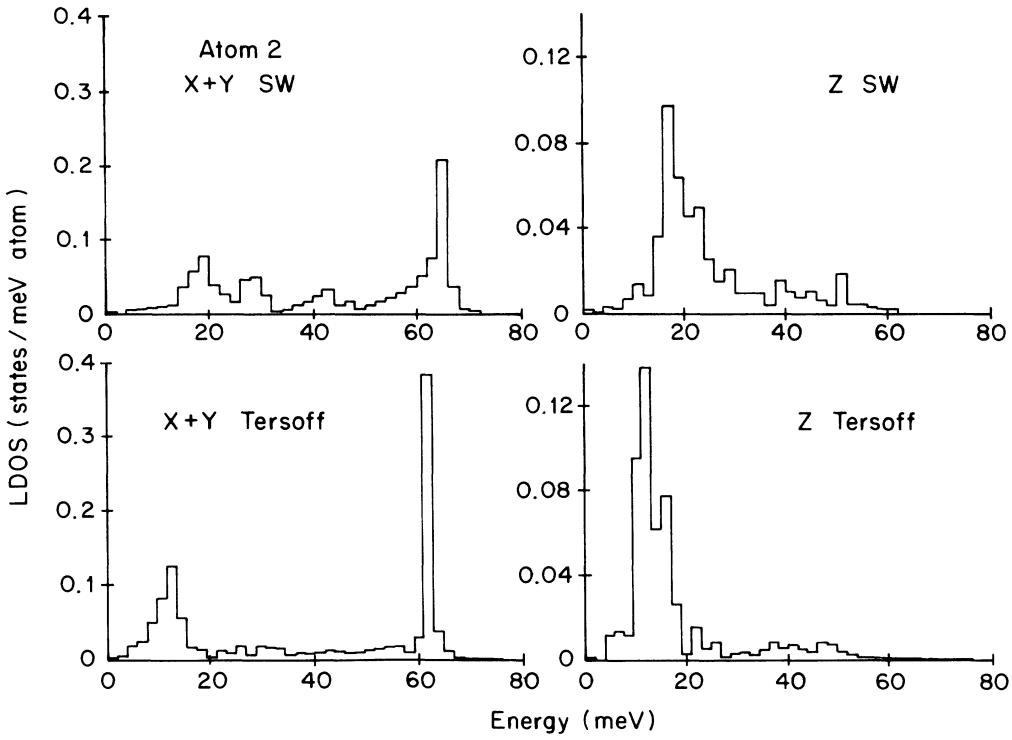

FIG. 8. Same as Fig. 7, but for atom 2 of Fig. 1 (a first-layer atom not attached to an adatom).

quencies for the two potentials into coincidence also brings those on most of the near-surface atoms into coincidence. Similarly, the mid-frequency–range DOS intensity is higher for the SW than for the Tersoff II potential. This effect spills over into most of the LDOS spectra of near-surface atoms. (A notable exception to this is given in the paragraph directly below.)

Lastly, we turn to the adatoms and the atoms to which they are attached. A typical LDOS spectrum is shown in Fig. 9 for the adatom labeled 3 in Fig. 1. Notice first the similarities. The x and y components have significant low-frequency weight. The z component shows a high-frequency split-off state near 76 meV for both potentials. Further, there is a mid-frequency–range state in the z component which shows up for both potentials. The big difference, however, is the complete absence of any coupling in the x and y components to high- and mid-frequency bulk modes for the SW potential. Our explanation of this observation is that the z separation of the adatoms in the relaxed DAS structure is so large that coupling to atoms other than nearest neighbors is poor. (See Tables V and VI.)

A representative example of the LDOS of a second-layer atom directly beneath an adatom is given in Fig. 10 for atom 4. Here the overall similarity between the results of the two potentials is striking. The (x,y) components show a significant intensity near 12 meV and a doublet in the (45–65)-meV range. The z component essentially shows only one resonance at 76 meV.

A spectrum representative of the first-layer atoms directly attached to adatoms (atom 5) is given in Fig. 11. Again, the features in the spectra are very similar. The high-frequency split-off state occurs only in the (x,y) components.

Lastly, consider the third-layer atoms directly beneath adatoms (atom 6). A representative spectrum is shown in Fig. 12. The (x,y) spectra of both potentials look very similar to their bulk spectra, implying that the influence of surface on this layer is already little in the (x,y) direction. However, the spectra show large effects of adatoms in the z direction. The high-energy split-off and mid-frequency structures are still there, as well as some features of the bulk phonons.

The mean-square displacement (MSD) of atom l in the polarization direction α can be calculated from our spectra:

$$\langle u_\alpha^2 \rangle = \sum_i \left[\frac{\hbar}{2M\omega_i} \right] | \varepsilon_i(l,\alpha) |^2 [2n(\omega_i)+1] , \quad (8)$$

where $n(\omega)$ is the Bose-Einstein distribution for phonons. MSD's are related to Debye-Waller factors and can be measured by x-ray-diffraction experiments. Table VII gives MSD's of the top few surface layers at 300 K compared with the experimental results of Robinson *et al.*[33] For the adatoms both potentials agree with the experimental observation of much larger MSD's on adatoms than in the bulk. For the double layer beneath the adatoms, we find MSD's only moderately larger than in the bulk, and marginally within the assigned experimental error. At room temperature the MSD's are dominated by low-frequency modes. Figures 3 and 5 show that the acoustic modes of the SW potential agree very well with experiment, except at the Brillouin-zone boundaries,

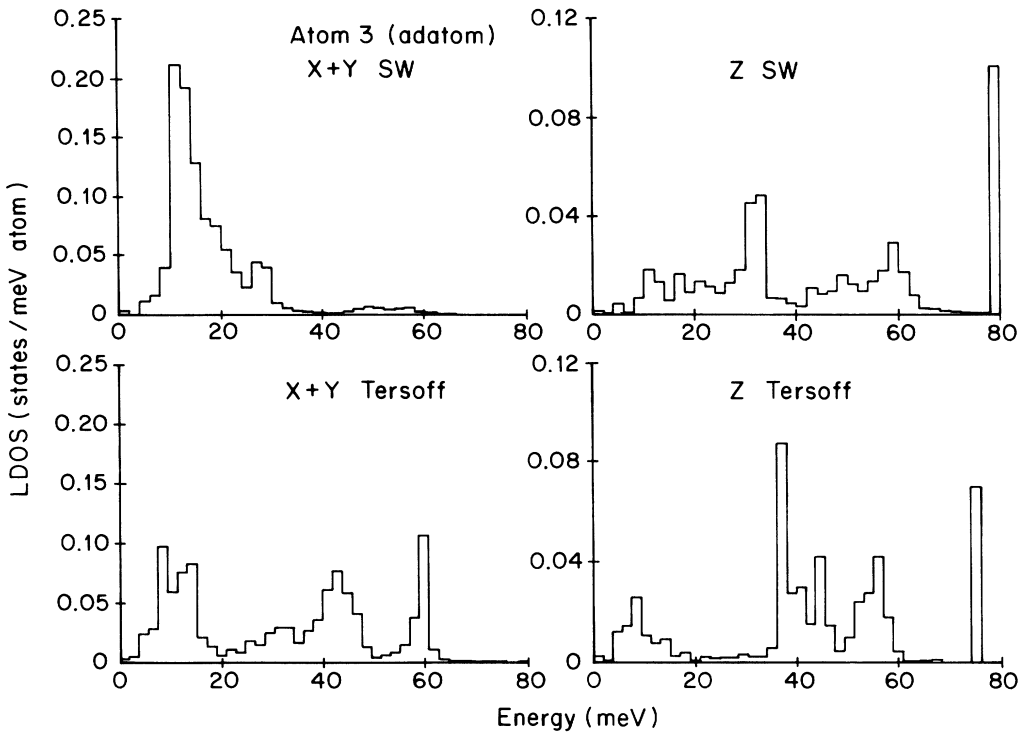

FIG. 9. Same as Fig. 7, but for atom 3 of Fig. 1 (an adatom).

whereas the Tersoff II potential significantly underestimates them. Thus we expect that the SW potential gives a good bulk MSD, but that the Tersoff II potential will overestimate it by a large amount. This is exactly the case compared with experiment.[34]

Before leaving this section we note a pathology with the Tersoff II potential. Examination of Eq. (4) and the constants given in Table I shows that b is very small and the exponent n is large. These two effects conspire to make B_{ij} vary rapidly over a narrow range of Z_{ij} values.

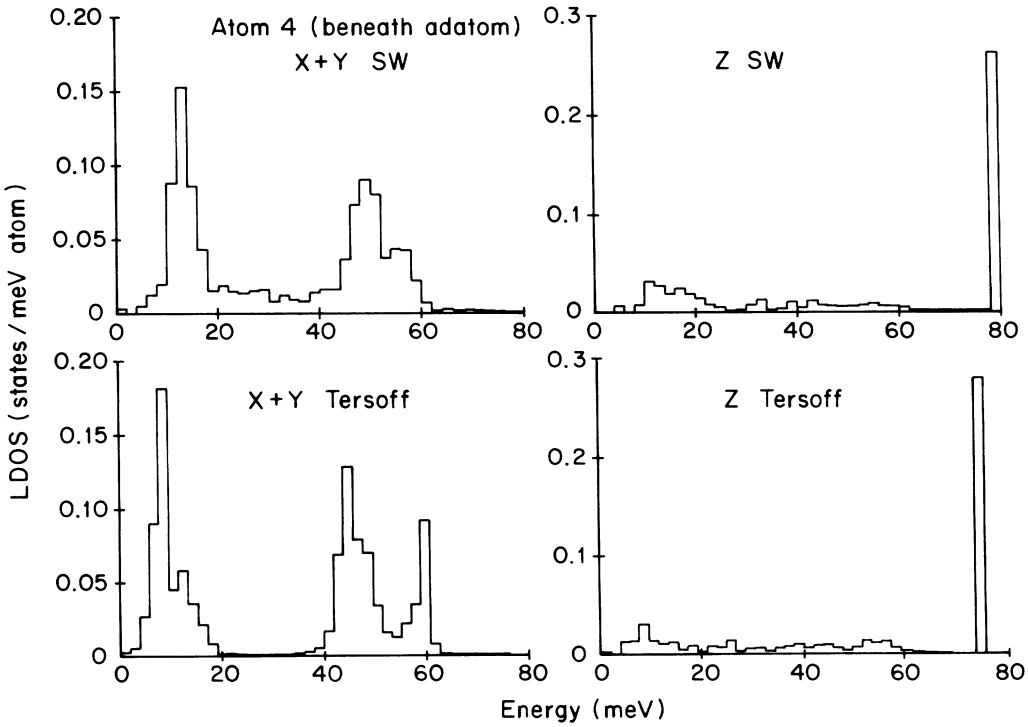

FIG. 10. Same as Fig. 7, but for atom 4 of Fig. 1 (directly below an adatom).

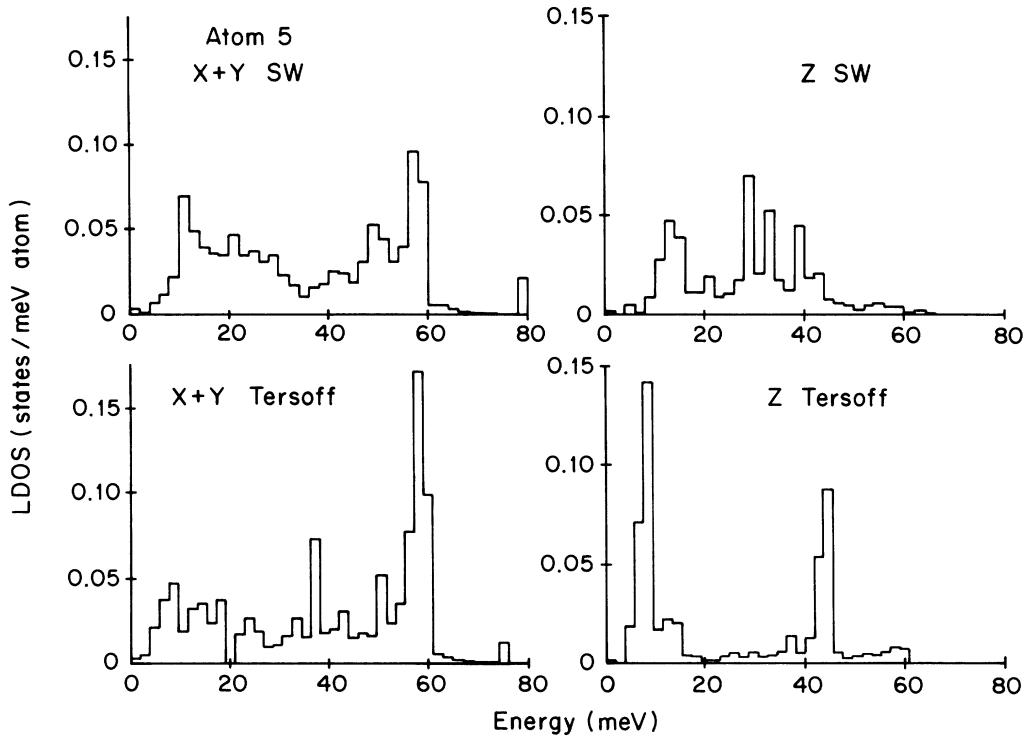

FIG. 11. Same as Fig. 7, but for atom 5 of Fig. 1 (a first-layer atom attached to an adatom).

The second derivative of B_{ij} with respect to Z_{ij}, which contributes to the values in the dynamical matrix, goes through a dramatic minimum over a narrow Z_{ij} range. If, in the energy- minimization process used to find a relaxed surface structure, a Z_{ij} value occurs in the relaxed state corresponding to one of these pathological Z values, then anomalously high frequencies may be observed after diagonalization of the dynamical matrix. As pointed out in the Introduction, the Tersoff potential employed here is not the original one (Tersoff I),[17] since the original has

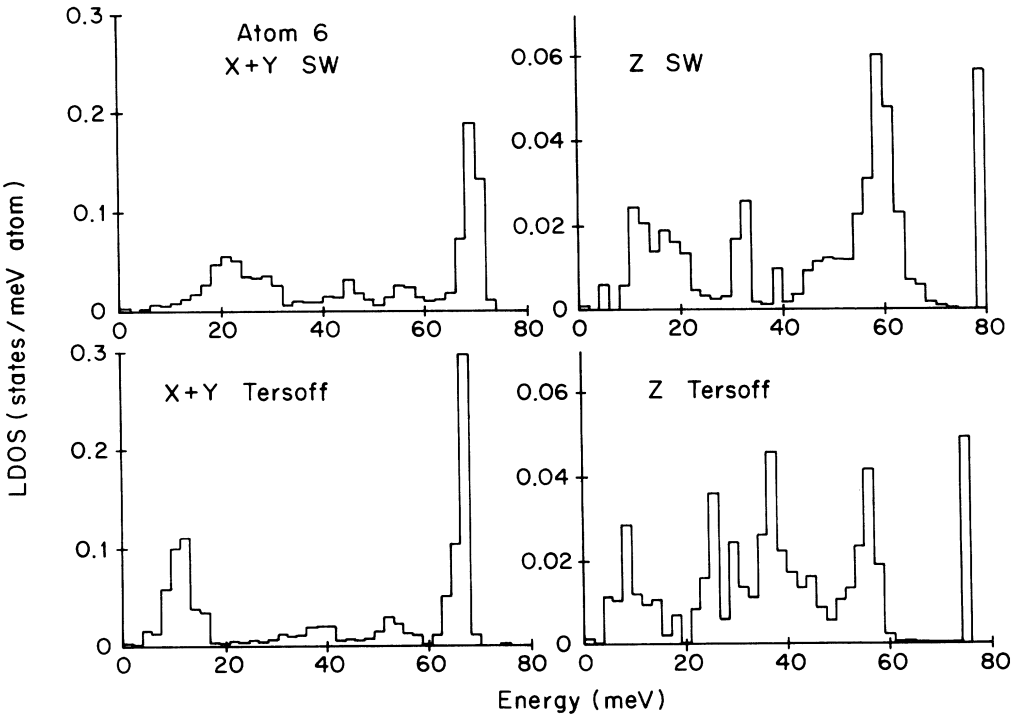

FIG. 12. Same as Fig. 7, but for atom 6 of Fig. 1 (a third-layer atom beneath an adatom).

TABLE VII. Mean-square displacements, $\frac{1}{2}\langle u_x^2+u_y^2\rangle$, in 10^{-2} Å of the top few surface layers at 300 K, averaged over all the atoms in the layer. The experimental results are from Ref. 33 and include the effects of static disorder.

Atom layer	SW potential	Tersoff II potential	Expt.
Adatoms	2.14	1.92	1.9(8)[a]
First layer	0.79	1.44	1.9(8)
Second layer	0.75	1.75	0.0(5)
Bulk	0.50	1.51	0.57[b]

[a]This number may be as large as 4 [I. K. Robinson (private communication)].
[b]From Ref. 34.

an incorrect bulk ground state. Rather, Tersoff II is a modification to circumvent the problem and it is this which we use here.[18] Tersoff's first suggestion had been to set λ_3 equal to λ_1. With these parameter values, the minimization procedure results in an adatom configuration in which Z_{ij} values arise with pathological consequences for the second derivative of B_{ij}. The adatom and those closely coupled to it have high-frequency split-off states at greater than *twice* the bulk frequency cutoff. This seemed unphysical. Tersoff's second suggestion was to set λ_3 equal to λ_2. Relaxation now produces almost identical energies and atomic positions to his first choice, but now the pathological region of B_{ij} is avoided and we obtain the results reported in this paper. Structures and low-order properties such as energy are insensitive to the choice of λ_3, but higher-order properties may be very sensitive if conditions conspire to produce unfortunate Z_{ij} values. Empirical potentials flexible enough to interpolate between elements of a diverse data base and immune to unphysical oscillations or kinks in between are difficult to devise.

V. COMPARISON WITH EXPERIMENT AND CONCLUSIONS

In spite of the fact that the SW and Tersoff II potentials yield quite different energies and relaxed coordinates, Figs. 7–12 show many similarities in their surface vibrations. No doubt this derives partly from constraints of symmetry and of the underlying bulk vibrations (which are similar for the two potentials). Therefore we are encouraged to believe that surface vibrations common to both models are robust and likely to be real. A recent electron-energy-loss–spectroscopy experiment by Daum *et al.*[24] seems to confirm this very nicely. They observed a sharp feature at 71 meV, above the top of the bulk-phonon spectrum (65 meV) by 10%. This corresponds precisely to the sharp feature at 79 meV of the SW model and at 75 meV of the Tersoff II model, $\approx 10\%$ above the top of the corresponding bulk spectra (73 and 69 meV, respectively). The experimental line shape corresponded to a totally symmetric vibration, and was attributed[24] (by means of an electronic-structure calculation for a cluster) to a z-polarized adatom vibration, coupled out of phase to z vibrations of the atom underneath, and to (x,y) vibrations of the three nearest-neighbor atoms. This agrees precisely with the spectra of Figs. 9–12, except that we find a significant weight of this high-energy mode on the third-layer atom beneath the adatom, which is not considered by the cluster calculations of Daum *et al.*[24] These atoms vibrate in phase with adatoms. The EELS also show a broader feature in the range 25–33 meV, attributed also to totally symmetric vibrations. It is striking that the adatom (Fig. 9) z vibrations show a peak in just this range (where bulk vibrations are fairly uncommon) for both potentials (even though the nearby TA phonons are described very differently by the two modes). The eigenvectors of these localized modes consist of in-phase z motions of the adatom and the two atoms underneath, and symmetric (x,y) breathing of the three nearest-neighbor atoms with a nearly equal amplitude of z motion out of phase with the adatom. Thus our calculations provide a confirmation and an extension of the interpretation of Daum *et al.*[24]

A prediction not yet confirmed is that surface atoms with dangling bonds (first-layer atoms not coupled to an adatom and the atom at the corner, as in Figs. 7 and 8) should show z vibrations of quite low energy (15–25 meV according to the SW potential and 10–20 meV according to the Tersoff II potential, the differences presumably reflecting the different treatment of TA bulk phonons). This feature is readily understood. When these atoms vibrate in the z direction, no bond is stretched. The force constant contributed completely from the bond bending is, therefore, very small, which gives only low vibrational frequencies. Both this feature and the adatoms vibrations already seen by electron-energy-loss spectroscopy could be looked for by inelastic-scanning-tunnelling microscopy, which is supposed to be sensitive to z-polarized vibrations.[35]

Finally, we reiterate that the energies given in Table II show that the SW potential is absolutely unreliable in predicting the relative stability of possible (111) surface structures, while the Tersoff II potential, although a great improvement, still has the $(\sqrt{3}\times\sqrt{3})$ H-site structure relatively far too stable. It is remarkable that vibrational properties are not more contaminated by these shortcomings.

ACKNOWLEDGMENTS

We thank J. Tersoff for helpful advice, for allowing us to use his potential II prior to publication, and for checking some of our calculations. We thank I. K. Robinson for informing us about his Debye-Waller–factor determinations. One of us (J.Q.B.) would like to thank the U. S. Department of Energy (DOE) for support (Grant No. DE-FG02-85ER45218); the other co-authors (X.P.L., G.C., and P.B.A.) thank the National Science Foundation (NSF) for support (Grant No. DMR-84-20308).

[1]G. Binnig, H. Rohrer, Ch. Gerber, and E. Weibel, Phys. Rev. Lett. **50**, 120 (1983).
[2]K. Takayanagi, Y. Tanishiro, M. Takahashi, and S. Takahashi, J. Vac. Sci. Technol. A **3**, 1502 (1985).
[3]I. K. Robinson, W. K. Waskiewicz, P. H. Fuoss, J. B. Stark, and P. A. Bennett, Phys. Rev. B **33**, 7013 (1986).
[4]R. J. Hamers, R. M. Tromp, and J. E. Demuth, Phys. Rev. Lett. **56**, 1972 (1986).
[5]R. S. Becker, J. A. Golovchenko, E. G. McRae, and B. S. Swartzentruber, Phys. Rev. Lett. **55**, 2028 (1985).
[6]W. A. Harrison, Surf. Sci. **55**, 1 (1976).
[7]J. E. Northrup, Phys. Rev. Lett. **53**, 683 (1984).
[8]J. M. Nicholls, P. Mårtensson, G. V. Hansson, and J. E. Northrup, Phys. Rev. B **32**, 1333 (1985).
[9]S. B. Zhang, M. L. Cohen, and J. E. Northrup, Surf. Sci. **157**, L303 (1985).
[10]J. E. Northrup, Phys. Rev. Lett. **57**, 154 (1986).
[11]J. E. Northrup and M. L. Cohen, Phys. Rev. B **29**, 1966 (1984).
[12]J. E. Northrup, in *Proceedings of the 18th International Conference on The Physics of Semiconductors, Stockholm, 1986,* edited by O. Engström (World Scientific, Singapore, 1986).
[13]Guo-Xin Qian and D. J. Chadi, J. Vac. Sci. Technol. B **4**, 1079 (1986); Phys. Rev. B **35**, 1288 (1987).
[14]P. N. Keating, Phys. Rev. **145**, 637 (1966).
[15]D. Vanderbilt, Phys. Rev. Lett. **59**, 1456 (1987); Phys. Rev. B **36**, 6209 (1987).
[16]F. H. Stillinger and T. A. Weber, Phys. Rev. B **31**, 5262 (1985).
[17]J. Tersoff, Phys. Rev. Lett. **56**, 632 (1986).
[18]J. Tersoff, Phys. Rev. B **37**, 6991 (1988).
[19]D. W. Drenner and B. J. Garrison, Phys. Rev. B **34**, 1304 (1986).
[20]E. M. Pearson, T. Halicioglu, and W. A. Tiller, J. Vac. Sci. Technol. A **5**, 293 (1987).
[21]R. Biswas and D. R. Hamann, Phys. Rev. Lett. **50**, 2001 (1985).
[22]S. Saito, S. Ohnishi, and S. Sugano, Phys. Rev. B **33**, 7036 (1986).
[23]K. E. Khor and S. Das Sarma Phys. Rev. B **36**, 7733 (1987).
[24]W. Daum, H. Ibach, and J. E. Müller, Phys. Rev. Lett. **59**, 1593 (1987).
[25]J. Q. Broughton and X. P. Li, Phys. Rev. B **35**, 9120 (1987).
[26]D. King and H. C. Anderson, Phys. Rev. B **34**, 6987 (1986).
[27]M. D. Khige and J. R. Ray (unpublished).
[28]M. T. Yin and M. L. Cohen, Phys. Rev. B **24**, 1303 (1981).
[29]B. W. Dodson, Phys. Rev. B **35**, 2795 (1987).
[30]T. A. Weber, in *Computer-Based Microscopic Description of the Structure and Properties of Materials,* Mater. Res. Soc. Symp. No. 63, edited by J. Q. Broughton, W. Krakow, and S. T. Pantelides (Materials Research Society, Pittsburgh, 1986).
[31]K. E. Khor and S. Das Sarma, Phys. Rev. B **36**, 7733 (1987).
[32]W. Weber, Phys. Rev. B **15**, 4789 (1977).
[33]I. K. Robinson, W. K. Waskiewicz, P. H. Fuoss, and L. J. Norton, Phys. Rev. B **37**, 4325 (1988).
[34]S. Gottlicher and E. Wolfel, Z. Elektrochem. **63**, 891 (1959).
[35]G. Binnig, N. Garcia, and H. Rohrer, Phys. Rev. B **32**, 1336 (1985).